Materials Chemistry and Physics 216 (2018) 136–142

Contents lists available at ScienceDirect

Materials Chemistry and Physics

journal homepage: www.elsevier.com/locate/matchemphys

Praseodymium doped ceria as electrolyte material for IT-SOFC applications

Irfana Shajahan[a], Junsung Ahn[b,1], Parvathi Nair[a,1], Srikar Medisetti[a], Sunaina Patil[a], V. Niveditha[a], G. Uday Bhaskar Babu[c], Hari Prasad Dasari[a,*], Jong-Ho Lee[b,**]

[a] Chemical Engineering Department, National Institute of Technology Karnataka, Mangalore 575025, India
[b] High-Temperature Energy Materials Research Center, Korea Institute of Science and Technology Hwarangno 14-gil 5, Seongbuk-gu, Seoul 136-791, South Korea
[c] Chemical Engineering Department, National Institute of Technology Warangal 506004, India

HIGHLIGHTS

- Praseodymium doped ceria (PDC) electrolyte was synthesised by EDTA citrate method.
- Dilatometer study revealed multiple shrinkage behaviour of PDC.
- PDC showed an ionic conductivity of 1.213E-03 S cm^{-1} at 700 °C.
- XRD at 1500 °C revealed that they crystallize as fluorite CeO_2 + cubic PrO_2 phase.

GRAPHICAL ABSTRACT

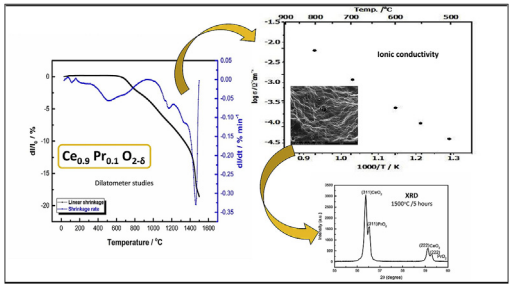

ARTICLE INFO

Keywords:
Fuel cells
Nanoparticles
Rare earth oxides
EDTA-Citrate method
Ceria
Dilatometer
Ionic conductivity
Sintering
IT-SOFC

ABSTRACT

Praseodymium-doped ceria (PDC, $Ce_{0.9}Pr_{0.1}O_2$) electrolyte material for intermediate temperature solid oxide fuel cells (IT-SOFCs) has been successfully synthesised by EDTA-citrate method. From X-Ray diffraction (XRD), fluorite structure along with a crystallite size of 5.4 nm is obtained for PDC nanopowder calcined at 350 °C/24 h. Raman spectroscopy confirmed the structure, presence of oxygen vacancies with the manifestation of the main peak at 457 cm^{-1} and with a secondary peak at 550 cm^{-1}. From Transmission Electron Microscopy (TEM) analysis, the average particle size is around 7–10 nm and selected area electron diffraction (SAED) patterns further confirmed the fluorite structure of PDC nanopowder. The PDC nanopowder displayed a BET surface area of 65 m^2/g with a primary particle size of ~13 nm (calculated from BET surface area). Dilatometer studies revealed a multi-step shrinkage behaviour with the multiple peaks at 522, 1171 and 1461 °C which may be originated due to the presence of multiple size hard agglomerates. The PDC electrolyte pellet sintered at 1500 °C displayed an ionic conductivity of 1.213E-03 S cm^{-1} along with an activation energy of 1.28eV. Instead of a single fluorite structure, XRD of sintered PDC pellet showed multiple structures (Fluorite structure (CeO_2) and cubic structure (PrO_2).

1. Introduction

Solid oxide fuel cells (SOFCs) are considered as a promising device for electrochemically converting a gaseous fuel in to useful energy with higher conversion efficiency and less environmental impact [1]. One of the main components of SOFC systems include dense solid oxide ion conducting ceramic electrolyte membrane sandwiched between cathode and anode. The well-known oxygen ion conducting ceramic

* Corresponding author.
** Corresponding author.
E-mail addresses: energyhari@nitk.edu.in (H.P. Dasari), jongho@kist.re.kr (J.-H. Lee).
[1] Equal contribution by the authors.

https://doi.org/10.1016/j.matchemphys.2018.05.078
Received 24 February 2018; Received in revised form 11 May 2018; Accepted 29 May 2018
Available online 30 May 2018
0254-0584/

electrolyte materials for SOFC includes cubic stabilized zirconia, doped cerium based oxides, bismuth based oxides and lanthanum gallate based oxides. Yttria stabilized zirconia is considered as the most preferred electrolyte material for SOFC at high temperatures because of its high ionic conductivity, high chemical and mechanical stability. But the disadvantage of this system is that higher operating temperature leads to high fabrication cost, mismatch in thermal expansion coefficient and causes reaction between the cell components [2]. Therefore, it becomes necessary to decrease the operating temperature and to develop electrolyte materials in the intermediate temperature range to commercialize the technology. Problems of lanthanum gallate oxide based electrolyte system sintered at higher temperature includes the volatilization of gallium(I) oxide (Ga_2O) from the perovskite structure and thereby reduces the overall ionic conductivity of the electrolyte material [3]. In spite of remarkably high ionic conductivity, bismuth oxide based electrolytes possess drawbacks such as thermodynamic, structural and chemical instability and pure bismuth oxide undergoes phase transformations from cubic to monoclinic on cooling below 730 °C resulting in a drop in ionic conductivity [4,5]. Among all these materials, rare-earth doped ceria has been found to be a promising electrolyte for IT-SOFCs operating at temperature lower than 700 °C [2,6–10].

Ceria based materials have found applications in various fields apart from SOFCs, such as oxygen sensors [11], catalyst/photo catalyst [12], UV blockers [13] and oxygen storage capacitors [13]. Apart from this, photo catalytic degradation of organic dyes using cerium oxide catalyst in UV/visible beams are considered as an effective way in removing the organic contaminants due to biodegradable nature of pollutants is yet another application of cerium oxide [14]. Since nano particles exhibit promising properties that are different from their relative bulk properties, cerium oxide nanoparticles has been widely used in many above mentioned applications mainly due to the low energy band gap between Ce^{3+} and Ce^{4+}, high mobility and also due to high oxygen storage capacity.

Rare earth doped ceria based materials possess lower activation energy and high ionic conductivity at relatively lower temperature as compared to YSZ electrolyte and show good promise in replacing state-of-the-art YSZ as the electrolyte materials. At 1000 °C, YSZ exhibit an ionic conductivity higher than 0.1 S cm^{-1} ; coefficients of thermal expansion similar to the other cell components, high ionic conductivities (> 0.1 S cm^{-1}) at intermediate temperatures, and chemical stability during cell operations are the important aspects to be considered for a ceramic material to be used as an electrolyte material [15]. Moreover, at lower temperatures the cell performance is decreased in case of YSZ material. Thus, ceria based ceramics are considered as the most promising electrolyte material for SOFC because of its high ionic conductivity which in turn reduces the operating temperature and eliminates the technical issues. The enhancement of ionic conductivity in doped ceria is mainly due to oxygen ion vacancies [6].

Some of the reports on Praseodymium-doped ceria materials (PDC) indicate that it can be a candidate for electrolyte materials for SOFCs [16,17]. Pr cation can exist in two oxidation states (Pr^{3+}/Pr^{4+}) and promote oxygen vacancies, and its presence in ceria lattice alters the grain boundary behaviour of the oxide system and thus enhances the conductivity [18,19]. For Pr doped ceria, the density of the anion vacancies is lower when compared to the other dopants like gadolinium and samarium, and this can be due to the presence of multi valance state [20]. A massive increase in chemical expansion upon heating is another critical anomalous behaviour of PDC [21], which can cause stoichiometric or phase change expansion. Above-mentioned desirable properties motivated the present study to explore/synthesise PDC nanopowder as an alternative electrolyte material for IT-SOFCs.

According to literature, PDC has been synthesised by variety of techniques such as hydrothermal method [22], sol gel method [23], flux method [24], co-precipitation method [25], combustion synthesis [17] etc. When compared to various synthesis methods, EDTA-citrate method is used to prepare a wide variety of oxide materials [26,27].

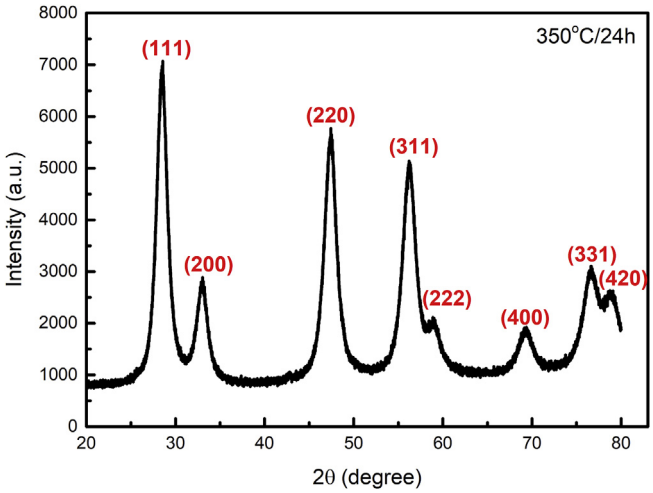

Fig. 1. XRD pattern of PDC sample calcined at 350 °C/24 h.

EDTA and citric acid are used as chelating agents, which forms stable complexes. EDTA citrate method offers the possibility for the synthesis of nano scaled particle size with good compositional homogeneity [28].

Nauer et al. [29] reported that cerium-praseodymium oxide forms fluorite-type solid solutions for all samples up to 30 mol% PrO_{2-x} while M. J. Chen et al. [30] obtained single phase fluorite solid solution up to 35 mol%. Wang et al. [16] noticed a decrease in cell parameter for 20-mol% Pr and indicated that the solubility limit for PDC might be around 20 mol%. These differences in regarding the solubility of Pr in CeO_2 may be due to differences in synthesis and processing procedures including the heat-treatment conditions [31]. According to literature several theoretical and experimental studies have suggested 10 mol% of gadolinium oxide and 10 mol% samarium oxide is the best dopant concentration for cerium dioxide to obtain high ionic conductivities [6,32–35]. In the present study, for Pr, a fixed amount of 10 mol% is taken and is synthesised by the EDTA-Citrate complexing method; and physical characterization along with dilatometer study and ionic conductivity measurements were carried out.

2. Experimental

2.1. Powder synthesis

AR grade chemicals Cerium nitrate hexahydrate ($Ce(NO_3)_3{\cdot}6H_2O$, SRL Chemicals ≥ 99%), Praseodymium nitrate hexahydrate ($Pr(NO_3)_3{\cdot}6H_2O$, Sigma Aldrich Chemicals 99%), EDTA (ethylenediaminetetraacetic acid, Sigma Aldrich Chemicals ≥ 99%) and citric acid (Sigma Aldrich Chemicals ≥ 99%), Ammonium hydroxide (NH_4OH, 25% ammonia Spectrum reagents)) were used for the synthesis of PDC nano-crystalline material by EDTA citrate complexing method. Stoichiometric amounts of Cerium nitrate hexahydrate and Praseodymium nitrate hexahydrate were dissolved in deionised water and the solution is stirred continuously at room temperature. EDTA and citric acid were used as chelating agents. The required amount of EDTA dissolved in NH_4OH for the complete dissolution was then added to the aqueous solution of metal nitrate. Stoichiometric amount of citric acid was added to the resulting solution under continuous stirring to allow citric acid to dissolve completely to obtain a clear solution. Then necessary amount of NH_4OH solution was added to the clear solution to maintain the pH (~9) to the desired value. The mole ratio of total metal ions to EDTA and to citric acid used was 1:1:1.5. After homogenisation of the solution, the resulting final solution was heated at 100 °C to remove excess water and nitrate gases under continuous stirring condition to obtain a thick, viscous gel. The gel obtained is kept in the hot air oven for 24 h at 150 °C temperature in order to convert it to a black

Table 1
Comparison of PDC material synthesised by various methods.

Synthesis method	Lattice Constant (Å)	Particle Size (nm)	BET Surface area (m^2/g)	Crystallite size (nm)[c]	Calcination Temperature (°C)	Reference
Hydrothermal method	5.450	13–25[b]	72	16.1	100/2 h	[36]
EDTA Citrate method	5.414	13[a]	65	5.4	350/24 h	[This study]
Combustion method	5.405	25[a]	34	17.1	700/2 h	[37]
Sol-gel method	5.413	30–50[b]	17	31.3	900/4 h	[23]

[a] Average particle size calculated from BET data.
[b] Average particle size calculated from TEM data.
[c] Crystallite size calculated from XRD data.

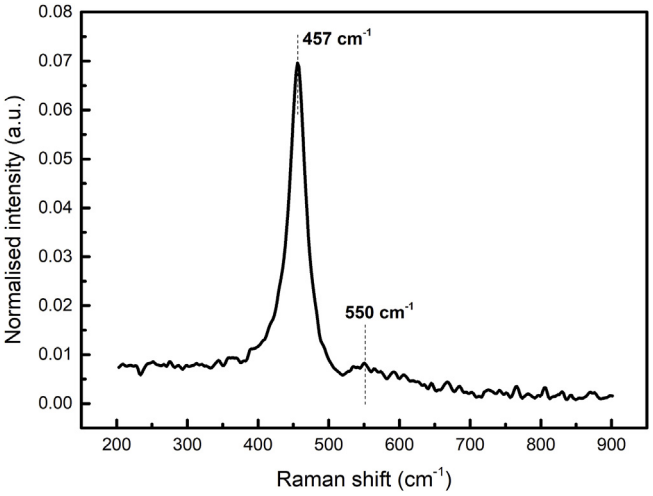

Fig. 2. Raman spectra of PDC sample calcined at 350 °C/24 h.

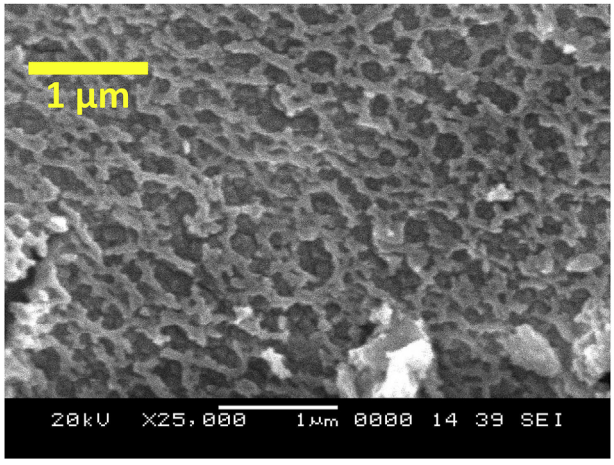

Fig. 3. SEM micrograph of PDC sample calcined at 350 °C/24 h.

solid precursor, was then ground and calcined at 350 °C/24 h to get the final metal oxide product.

2.2. Powder characterization

The obtained PDC nanopowder after calcination was subjected to various powder characterization techniques. The phase analysis and crystal structure and of the synthesised nano powder were done by using XPERT-PRO diffractometer with Cu Kα radiation (λ = 1.540498 Å) operated at 40 kV and 30 mA in the 2θ range of 20–80° with a step size of 0.02 and a time for step is 2s. Debye – Scherer equation was used to calculate the crystallite size of the nano particles and is given by:

$$d = (0.9\lambda)/(\beta \cos \theta),$$

Where, λ is the wavelength of X–rays, β is the full width at half maximum intensity and θ is the angle of main reflection (111).

Raman spectroscopic studies were done using BRUKER - RFS27 FT-Raman spectrometer to further analyze the phase and the presence of functional molecules in the materials. JSM-6380LA Scanning Electron Microscope was used to study the surface morphologies of the obtained powder. To view the inner texture of the particle, analysis was carried out using JEM 2100, JEOL TEM (Transmission Electron Microscope) along with SAED (Selective Area Electron Diffraction). SMARTSORB—92/93 instrument was used to measure the BET surface area. In order to remove the residual moisture, the samples were evacuated at 150 °C/3 h before the analysis and nitrogen gas was flushed for 2 h.

The dilatometric studies were carried out on the sample calcined at 600 °C/5 h. The shrinkage behaviour was examined using dilatometer measurement (Netzsch Dil 402C/3/G) at a heating rate of 3 °C min^{-1} from 50 °C to 1500 °C in air. The conductivity of the sintered pellet was obtained by four probe method by applying platinum paste to the other two ends of the pellet to form the electrodes. For measuring the conductivity data, the calcined samples were pelletized and heat-treated at 1500 °C/5 h with a heating rate of 3 °C min^{-1}, and the flow rate of air was maintained at 50 ml/min. The ionic conductivity measurements was carried out by four-probe DC method from 600 °C to 850 °C using the precision current source (Keithley 6220, USA) and the multimeter (Keithley2000, USA).

3. Results and discussion

3.1. X-ray analysis

XRD patterns of the PDC nanopowder calcined at 350 °C for 24 h is shown in Fig. 1. The relatively broad peaks would indicate the presence of a crystalline phase and the formed crystallites was very small. From the XRD pattern of the calcined PDC nanopowder, all the major peaks obtained correspond to the typical of crystalline CeO_2 with cubic fluorite like structure and matches with the JCPDS card data no. 34–0394 [22,36,37]. The average crystallite size as calculated by Debye Scherrer's equation of the most intense peak (111) was found to be 5.44 nm, which matches the value observed from TEM. The average value of lattice constant calculated using Bragg's equation was 0.5414 nm. Table 1 shows various physical parameters of PDC nanopowder synthesised by hydrothermal synthesis [36], combustion method [37], sol-gel method [23]. Table 1is arranged in the increasing order of the calcination temperature (from 100 to 900 °C). As it can be noticed from Table 1, there is an increase in the particle size, decrease in the BET surface area with an increase in the calcination temperature. It is interesting to note from Table 1 that the crystallite size did not follow the similar trend. The crystallite size (5.4 nm) of PDC nanopowder obtained from the current study (EDTA Citrate method, calcined at 350 °C/24 h) is smaller (5.4 nm) than the crystallite size (16.1 nm) obtained by the hydrothermal method, calcined at 100 °C/2 h). It shows that the synthesis method plays a crucial role in controlling the powder characteristics such as crystallite size, morphology,

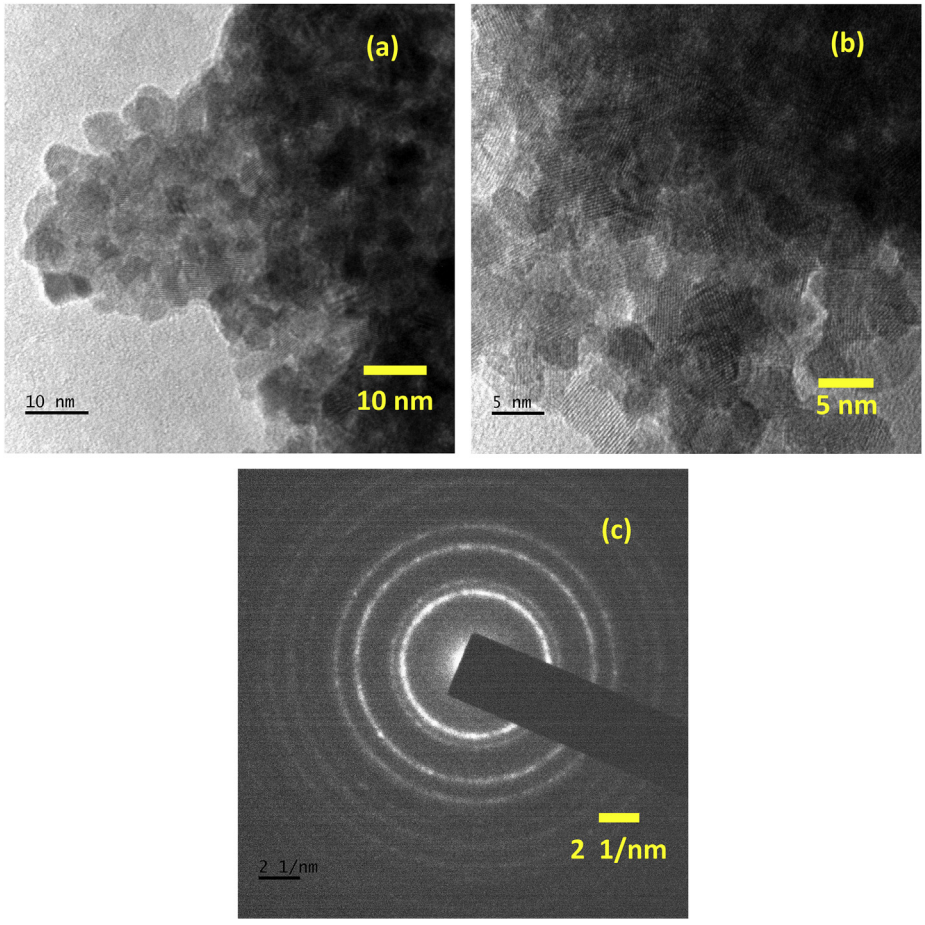

Fig. 4. (a) and (b) TEM micrographs of the calcined PDC powder (350 °C/24 h) and (c) SAED patterns for calcined PDC nanopowder.

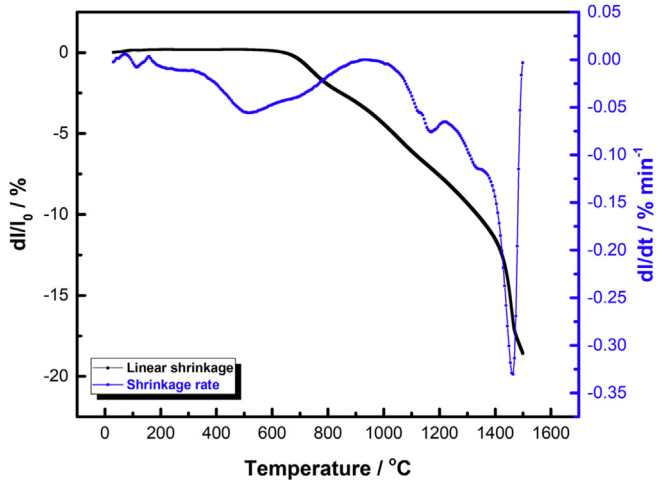

Fig. 5. Linear shrinkage and shrinkage rate of PDC green pellet from 50 °C to 1500 °C. (For interpretation of the references to colour in this figure legend, the reader is referred to the Web version of this article.)

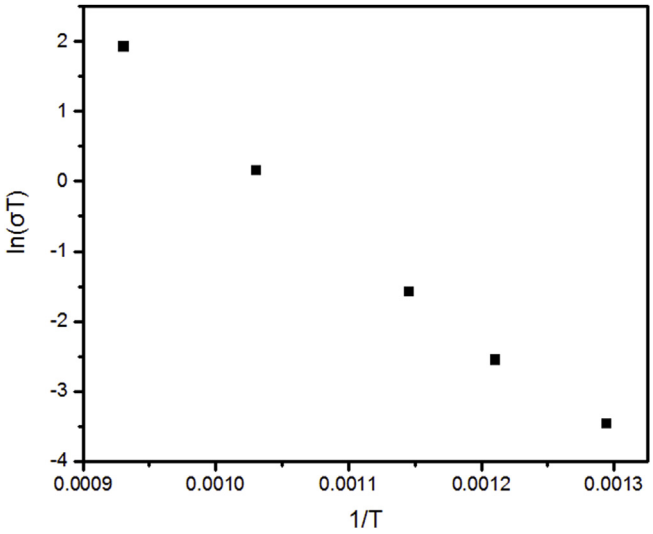

Fig. 6. Ionic conductivity of PDC pellet sintered at 1500 °C/5 h.

agglomeration and surface area of the PDC nanopowder. With the developed PDC material with small crystallite size and high BET surface area it could be used in other applications like dye degradation and antibacterial activity applications [12,38–40].

The reaction between stoichiometric metallic salts in a mixed solution which attributes to the band tail effect is related to intrinsic defects is one of the advantages of the present method. Peng et al. [41] reported that the smaller particle size of the materials allows the sintering of the material into highly dense ceramic pellets at a significantly lower sintering temperature. It was also reported that the powder with highest surface area and smaller particle size allows high sintered density at a lower temperature in a short time [42]. Smaller pore requires relatively lower temperature to close the pores whereas larger pores require a higher temperature and longer time to eliminate the pores. Thus the formation of smaller particle size with soft nature of agglomerates decreases the sintering temperature compared to hard

Table 2
Comparison of Ionic Conductivity of 10-mol% PDC material obtained by various synthesis methods.

Synthesis method	Total Conductivity at 700 °C (S/cm)	Activation Energy (eV)	Sintering Temperature (°C)	Reference
Hydrothermal Method	6.6×10^{-4}	1.20	1300/4 h	[22]
EDTA-Citrate Method	1.2×10^{-3}	1.28	1500/5 h	[This study]
Pechini Method	1.1×10^{-2}	–	1500/14 h	[30]

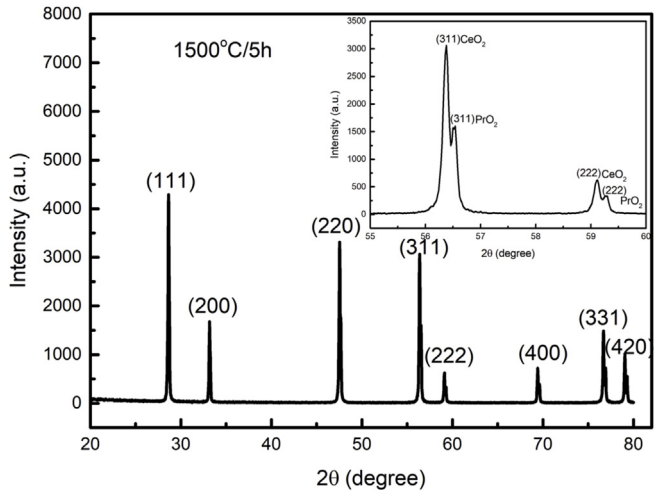

Fig. 7. XRD pattern of PDC sample sintered at 1500 °C/5 h.

nature of agglomerates with wider pore distribution [43]. Thus the powder characteristics affect the densification process during sintering, which will be discussed in-detail in the dilatometer studies in section 3.4.

3.2. Raman spectra analysis

Fig. 2 represents the Raman spectra of the PDC powder synthesised by the EDTA - citrate method, which confirms the formation of cubic fluorite phase shown in Fig. 1. An intense and sharp peak at 457 cm^{-1} was observed and can be attributed to F_{2g} vibration mode (O-Ce-O) of the fluorite-like structure of pure CeO_2 [17,44]. Besides, an additional weak intense peak at 550 cm^{-1} was observed, and it can be associated to a band that could be due to the extrinsic oxygen vacancies present in the solid solution [45]. The changes in the Raman spectra are related to O vacancies introduced into the cation lattice (multivalent Pr is substituted for Ce^{+4}). Since the radius of Pr^{3+} is larger than Ce^{4+}, it is expected to cause an expansion of the CeO_2 lattice. At higher temperatures, the migration of oxygen ions is facilitated by the presence of oxygen vacancies and thus enhances the ionic conductivity. Since the oxygen vacancies facilitate the migration of oxygen ions through the crystal lattice that also enhances the low temperature densification during sintering [46]. Thus, the results from the literature suggest that the ionic conductivity of the sample is enhanced by the presence of high concentration of oxygen vacancies [47]. From the Raman spectroscopy analysis, no indications can be found regarding the presence of an impurity phase even after the calcination step, which is in good agreement with the XRD analysis.

3.3. SEM and TEM analysis

SEM microstructure of the PDC nanopowder are shown in Fig. 3. It is observed that the PDC electrolyte material synthesised is very porous in nature and exhibit particle agglomeration up to a certain extent. Fig. 4 (a) and 4(b) depicts the TEM image of the PDC nanoparticles. Spherically shaped particles with slight agglomeration were observed. Fig. 4(c) shows the corresponding selected area electron diffraction (SAED) patterns of PDC nanopowder. The figure shows concentric rings, which is attributed to (1 1 1), (2 0 0), (2 2 0) and (3 1 1) reflections and these patterns indexed to the cubic fluorite structure of PDC nanopowder matches well with the XRD results.

3.4. Dilatometry studies

The shrinkage rate spectra and linear shrinkage of the PDC pellet is shown in Fig. 5. The sintering process of PDC sample undergoes multiple step shrinkage behaviour is evident from the figure. The shrinkage maxima at 522, 1171 and 1461 °C indicates the presence of multiple size hard agglomerates after compaction [48]. This can be attributed to the shrinkage of different pore sizes in between the hard agglomerates obtained from the non-uniform particle size distribution (please check the supplementary information Fig.S1 for non-uniform particle size distribution of calcined PDC powder). From the linear shrinkage of PDC sample as shown in Fig. 5, the shrinkage has not fully completed below 1500 °C with a final linear shrinkage of 18%. From dilatometer studies obtained for PDC pellet, it is confirmed that the synthesis method and/or processing conditions have to be altered to achieve nanoparticles with uniform particle size distribution, which leads to uniform shrinkage behaviour and thus decreases the sintering temperature of the PDC material. This will be one of the future goals to use this material as an electrolyte material for SOFC applications.

3.5. Conductivity measurements

Fig. 6 manifests the Arrhenius plot of the conductivity obtained from the PDC pellet sintered at 1500 °C/5 h in the air. A linear increase in the conductivity is observed with the rise of the operating temperature from 500 °C to 800 °C.At 700 °C, the conductivity is 1.213E-03 $\Omega^{-1}cm^{-1}$ and is higher than the conductivity of the PDC pellet observed by Shuk and Greenblatt [22]. The activation energy obtained from the Arrhenius plot is around 1.28 eV. Table 2 shows the conductivity of the 10 mol% PDC materials synthesised by various methods. It is noticed that the conductivity is affected by the synthesis method (since synthesis method affects the powder properties) and when compared to the 10 mol% PDC conductivity obtained by MJ Chen et al. [30], the conductivity observed in the present study is low. The difference in the conductivities can be due to various factors; grain and grain boundary conditions, impurities, phase stability and charging effects. From the literature [49–54], metal tunnel junctions, single-electron charging effects studied in granular films and STM-grain junctions it become apparent that the transport properties of semiconductor submicron structures weakly coupled to the contact leads by tunnel barriers are strongly affected by the charging effects. The conductance oscillations in disordered wires triggered the study of charging effects in semiconductor devices and found that this oscillations are due to confinement of electron charges impurity potential barriers [49–52]. For finding out the reasons behind this behaviour, XRD analysis of the sintered PDC pellet is done and depicted in Fig. 7. From Fig. 7, it is evident that there is a clear phase separation (fluorite CeO_2 + cubic PrO_2) [55]. The observed diffraction peaks of ceria agree with the JCPDS card no. 34–0394 and the diffraction peaks of PrO_2 agrees well with the JCPDS card no. 00-024-1006 [55]. This phase separation might be the reason for showing a lower conductivity. The conductivity of 10 mol% PDC is one order lower than the 10 mol% GDC electrolyte material [56], and one of the reasons for such kind of low conductivity might be occurring due to phase separation of PDC material. In the band gap presence of shallow traps has to be identified in order to further enhance the conductivity. Thus the presence of shallow traps in the band gap affects the electrical property of the material as it

affects the transport of excitons and charge carriers in the lattice [57]. Thus, identification of the electron and hole traps are essential to control the electrical properties.

Apart from single element doped ceria, several researches have reported an enhancement in ionic conductivity of ceria by double or co-doping chemistry. When compared to the results of triple (Sm^{3+}, Pr^{3+} and Nd^{3+}) doped ceria obtained by Liu et al. the conductivity of PDC electrolyte material of the present study is lower than the ionic conductivity they have reported (0.125 S cm^{-1} at 600 °C). It was reported that the enhancement in ionic conductivity is due to the secondary doping of Pr^{3+} and Nd^{3+} ions which promote the surface oxygen transfer and enhance the grain boundary conductivity [58]. The ionic conductivity of the PDC material of the present study is less than that of nanocrystalline tri-doped ceria ($Ce_{0.76}Pr_{0.08}Sm_{0.08}Gd_{0.08}O_{2-\delta}$) synthesised by sol-gel auto combustion method (total ionic conductivity = 1.86×10^{-2} S cm^{-1} at 600 °C) reported by venkataramana et al. [59]. The high ionic conductivity of these samples is due to the presence of increase in concentration of oxygen vacancies/mobile ions in the sample.

To make PDC materials as an electrolyte material for SOF/EC applications further research work should be dedicated to finding new methods (synthesis, processing conditions and dopant modification) to reduce sintering temperature and enhance the ionic conductivity. Thereby overcoming the phase separation issue, which plays a crucial role in enhancing the ionic conductivity of the PDC electrolyte material for SOFC applications.

4. Conclusion

In summary, present study reports the characterization of PDC electrolyte material synthesised by EDTA citrate method. XRD and Raman spectroscopy analysis confirm that the calcined sample displayed a cubic fluorite structure. The bands at 457 cm^{-1} and 550 cm^{-1} in the Raman spectroscopy results confirmed the formation of PDC solid solution which is in good agreement with the XRD data. From XRD, BET and TEM analysis it can be observed that the calcined sample exhibited a crystallite/particle size of 5–10 nm and from particle size analyser, it is found that the sample displayed an agglomerate size 3.06 μm. From dilatometer studies, multi-step shrinkage behaviour is noticed for the PDC green pellet, a linear shrinkage up to −18% is noticed below 1500 °C. At 700 °C, the sample displayed conductivity of 1.213E-03 S cm^{-1} and with an activation energy of 1.28 eV. The result presented in the present paper indicates that a phase change of sintered PDC pellet occurs at 1500 °C. Forthcoming paper would be positioned on identification of the solubility limit of PDC material which plays a key role in enhancing the ionic conductivity and to decrease the sintering temperature of praseodymium doped ceria material below the solubility limit temperature, as an electrolyte material for IT – SOFCs.

Acknowledgements

This work was supported by KIST-IRDA alumni Project (Grant No. 2Z04820-16-095), Technology Develpoment Program to Solve Climate Changes through the National Research Foundation of Korea(NRF) funded by the Ministry of Science, ICT (NRF-2016M1A2A2940148) and DST-SERB-Early Career Research Award (Grant No. ECR/2016/002010ES). One of the authors (IS) would like to thank NITK for giving the opportunity to do PhD with a full scholarship. We would like to thank DST and sophisticated analytical instrument facility (SAIF) at India Institute of Technology (IIT) Madras for providing Raman data of our samples using FT-Raman spectrometer (Bruker FRS) instrument.

Appendix A. Supplementary data

Supplementary data related to this article can be found at http://dx.doi.org/10.1016/j.matchemphys.2018.05.078.

Authors' contribution

IS, PN and NV obtained all the experimental data. SM and SP contributed to material synthesis. UBB provided XRD data. HPD conceived the study. IS, PN, NV, HPD and JHL analysed all the experimental data, and all authors contributed to writing and editing the document.

References

[1] S.P.S. Badwal, K. Foger, Solid oxide electrolyte fuel cell review, Ceram. Int. 22 (1996) 257–265.
[2] H. Inaba, H. Tagawa, Ceria-based solid electrolytes, Solid State Ionics 83 (1996) 1–16, http://dx.doi.org/10.1016/0167-2738(95)00229-4.
[3] J.W. Stevenson, T.R. Armstrong, L.R. Pederson, J. Li, C.A. Lewinsohn, S. Baskaran, Effect of A-site cation nonstoichiometry on the properties of doped lanthanum gallate, Solid State Ionics 113–115 (1998) 571–583, http://dx.doi.org/10.1016/S0167-2738(98)00324-5.
[4] T. Takahashi, T. Esaka, H. Iwahara, Electrical conduction in the sintered oxides of the system Bi2O3-BaO, J. Solid State Chem. 16 (1976) 317–323, http://dx.doi.org/10.1016/0022-4596(76)90047-5.
[5] N. Jiang, E.D. Wachsman, Structural stability and conductivity of phase-stabilized cubic bismuth oxides, J. Am. Ceram. Soc. 82 (1999) 3057–3064, http://dx.doi.org/10.1111/j.1151-2916.1999.tb02202.x.
[6] B.C.H. Steele, Appraisal of Ce1 − yGdyO2 − y/2 electrolytes for IT-SOFC operation at 500°C, Solid State Ionics 129 (2000) 95–110, http://dx.doi.org/10.1016/S0167-2738(99)00319-7.
[7] G. Balazs, Ac impedance studies of rare earth oxide doped ceria, Solid State Ionics 76 (1995) 155–162, http://dx.doi.org/10.1016/0167-2738(94)00242-K.
[8] S.P.S. Badwal, F.T. Ciacchi, J. Drennan, Investigation of the stability of ceria-gadolinia electrolytes in solid oxide fuel cell environments, Solid State Ionics 121 (1999) 253–262, http://dx.doi.org/10.1016/S0167-2738(99)00044-2.
[9] G.B. Jung, T.J. Huang, M.H. Huang, C.L. Chang, Preparation of samaria-doped ceria for solid-oxide fuel cell electrolyte by a modified sol-gel method, J. Mater. Sci. 36 (2001) 5839–5844, http://dx.doi.org/10.1023/A:1012964307388.
[10] T. Mori, J. Drennan, J.H. Lee, J.G. Li, T. Ikegami, Oxide ionic conductivity and microstructures of Sm- or La-doped CeO2-based systems, Solid State Ionics 154–155 (2002) 461–466, http://dx.doi.org/10.1016/S0167-2738(02)00483-6.
[11] N. Izu, N. Murayama, W. Shin, I. Matsubara, S. Kanzaki, Resistive oxygen sensors using cerium oxide thin films prepared by metal organic chemical vapor deposition and sputtering, Jpn. J. Appl. Phys. 1 (43) (2004) 6920–6924, http://dx.doi.org/10.1143/JJAP.43.6920.
[12] C.M. Magdalane, K. Kaviyarasu, J.J. Vijaya, B. Siddhardha, B. Jeyaraj, Facile synthesis of heterostructured cerium oxide/yttrium oxide nanocomposite in UV light induced photocatalytic degradation and catalytic reduction : synergistic effect of antimicrobial studies, J. Photochem. Photobiol. B Biol. 173 (2017) 23–34, http://dx.doi.org/10.1016/j.jphotobiol.2017.05.024.
[13] K. Lin, S. Chowdhury, Synthesis, characterization, and application of 1-D cerium oxide Nanomaterials : a review, Int. J. Mol. Sci. 11 (2010) 3226–3251, http://dx.doi.org/10.3390/ijms11093226.
[14] C.M. Magdalane, K. Kaviyarasu, J.J. Vijaya, C. Jayakumar, M. Maaza, B. Jeyaraj, Photocatalytic degradation effect of malachite green and catalytic hydrogenation by UV – illuminated CeO 2/CdO multilayered nanoplatelet arrays : investigation of antifungal and antimicrobial activities, J. Photochem. Photobiol. B Biol. 169 (2017) 110–123, http://dx.doi.org/10.1016/j.jphotobiol.2017.03.008.
[15] X.J. Chen, K.A. Khor, S.H. Chan, L.G. Yu, Influence of microstructure on the ionic conductivity of yttria-stabilized zirconia electrolyte, Mater. Sci. Eng., A 335 (2002) 246–252, http://dx.doi.org/10.1016/S0921-5093(01)01935-9.
[16] Y. Kuru, S.R. Bishop, J.J. Kim, B. Yildiz, H.L. Tuller, Chemomechanical properties and microstructural stability of nanocrystalline Pr-doped ceria : an in situ X-ray diffraction investigation, Solid State Ionics 193 (2011) 1–4, http://dx.doi.org/10.1016/j.ssi.2011.04.012.
[17] C. Esther Jeyanthi, R. Siddheswaran, P. Kumar, M. Karl Chinnu, K. Rajarajan, R. Jayavel, Investigation on synthesis, structure, morphology, spectroscopic and electrochemical studies of praseodymium-doped ceria nanoparticles by combustion method, Mater. Chem. Phys. 151 (2015) 22–28, http://dx.doi.org/10.1016/j.matchemphys.2014.10.001.
[18] B.M. Reddy, G. Thrimurthulu, L. Katta, Y. Yamada, S.E. Park, Structural characteristics and catalytic activity of nanocrystalline ceria-praseodymia solid solutions, J. Phys. Chem. C 113 (2009) 15882–15890, http://dx.doi.org/10.1021/jp903644y.
[19] Y. Ji, J. Liu, T. He, J. Wang, W. Su, The effect of Pr co-dopant on the performance of solid oxide fuel cells with Sm-doped ceria electrolyte, J. Alloy. Comp. 389 (2005) 317–322, http://dx.doi.org/10.1016/j.jallcom.2004.08.018.
[20] V.A. Sadykov, T.G. Kuznetsova, Y. V Frolova-Borchert, G.M. Alikina, A.I. Lukashevich, V.A. Rogov, V.S. Muzykantov, L.G. Pinaeva, E.M. Sadovskaya, Y.A. Ivanova, E.A. Paukshtis, N. V Mezentseva, L.C. Batuev, V.N. Parmon, S. Neophytides, E. Kemnitz, K. Scheurell, C. Mirodatos, A.C. van Veen, Fuel-rich methane combustion : role of the Pt dispersion and oxygen mobility in a fluorite-like complex oxide support, Catal. Today 117 (2006) 475–483, http://dx.doi.org/10.1016/j.cattod.2006.06.017.
[21] S.R. Bishop, D. Marrocchelli, C. Chatzichristodoulou, N.H. Perry, M.B. Mogensen, H.L. Tuller, E.D. Wachsman, Chemical expansion: implications for electrochemical energy storage and conversion devices, Annu. Rev. Mater. Res. 44 (2014) 205–239,

http://dx.doi.org/10.1146/annurev-matsci-070813-113329.
[22] P. Shuk, M. Greenblatt, Hydrothermal synthesis and properties of mixed conductors based on Ce1−xPrxO2−δ solid solutions, Solid State Ionics 116 (1999) 217–223, http://dx.doi.org/10.1016/S0167-2738(98)00345-2.
[23] M. Guo, J. Lu, Y. Wu, Y. Wang, M. Luo, UV and Visible Raman Studies of Oxygen Vacancies in Rare-Earth-Doped Ceria, (2011), pp. 3872–3877.
[24] F. Bondioli, A.B. Corradi, T. Manfredini, C. Leonelli, R. Bertoncello, Nonconventional synthesis of praseodymium-doped ceria by flux method, Chem. Mater. 12 (2000) 324–330, http://dx.doi.org/10.1021/cm990128j.
[25] B.M. Reddy, G. Thrimurthulu, L. Katta, S. Park, Structural Characteristics and Catalytic Activity of Nanocrystalline Ceria - Praseodymia Solid Solutions, (2009), pp. 15882–15890.
[26] Z. Shao, S.M. Haile, A high-performance cathode for the next generation of solid-oxide fuel cells., Nature 431 (2004) 170–173, http://dx.doi.org/10.1038/nature02863.
[27] Z. Shao, W. Yang, Y. Cong, H. Dong, J. Tong, G. Xiong, Investigation of the permeation behavior and stability of a Ba0.5Sr0.5Co0.8Fe0.2O(3-δ) oxygen membrane, J. Membr. Sci. 172 (2000) 177–188, http://dx.doi.org/10.1016/S0376-7388(00)00337-9.
[28] D.H. Prasad, S.Y. Park, E.O. Oh, H. Ji, H.R. Kim, K.J. Yoon, J.W. Son, J.H. Lee, Synthesis of nano-crystalline La1-xSrxCoO 3-δ perovskite oxides by EDTA-citrate complexing process and its catalytic activity for soot oxidation, Appl. Catal. Gen. 447–448 (2012) 100–106, http://dx.doi.org/10.1016/j.apcata.2012.09.008.
[29] M. Nauer, B.C.H. Steele, An evaluation of Ce-Pr oxides and Ce-Pr-Nb oxides mixed conductors for cathodes of solid oxide fuel Cells : structure, thermal expansion and electrical conductivity, J. Electrochem. Soc. 14 (1994) 493–499.
[30] M.-J. Chen, S. Cheng, F.-Y. Wang, J.F. Lee, Y.L. Tai, Study of Pr-doped ceria-based electrolytes for ITSOFC, ECS Trans. 7 (2007) 2245–2252, http://dx.doi.org/10.1149/1.2729341.
[31] Y. Wang, T. Mori, J.-G. Li, T. Ikegami, Low-temperature synthesis of praseodymium-doped ceria nanopowders, J. Am. Ceram. Soc. 85 (2002) 3105–3107, http://dx.doi.org/10.1111/j.1151-2916.2002.tb00591.x.
[32] M. Mogensen, N.M. Sammes, G.A. Tompsett, Physical, chemical and electrochemical properties of pure and doped ceria, Solid State Ionics 129 (2000) 63–94, http://dx.doi.org/10.1016/S0167-2738(99)00318-5.
[33] L. Minervini, M.O. Zacate, R.W. Grimes, Defect Cluster Formation in M2 O3 -doped CeO2 vol. 116, (1999), pp. 339–349.
[34] H. Inaba, R. Sagawa, H. Hayashi, K. Kawamura, Molecular dynamics simulation of gadolinia-doped ceria, Solid State Ionics 122 (1999) 95–103.
[35] A. Arabaci, Effect of Sm and Gd dopants on structural characteristics and ionic conductivity of ceria, Ceram. Int. 41 (2015) 5836–5842, http://dx.doi.org/10.1016/j.ceramint.2015.01.013.
[36] A.I.Y. Tok, S.W. Du, F.Y.C. Boey, W.K. Chong, Hydrothermal synthesis and characterization of rare earth doped ceria nanoparticles, Mater. Sci. Eng., A 466 (2007) 223–229, http://dx.doi.org/10.1016/j.msea.2007.02.083.
[37] M. Jamshidijam, R.V. Mangalaraja, A. Akbari-fakhrabadi, S. Ananthakumar, S.H. Chan, Effect of rare earth dopants on structural characteristics of nanoceria synthesized by combustion method, Powder Technol. 253 (2014) 304–310, http://dx.doi.org/10.1016/j.powtec.2013.10.032.
[38] K. Kaviyarasu, L. Kotsedi, A. Simo, X. Fuku, G.T. Mola, J. Kennedy, M. Maaza, Photocatalytic activity of ZrO 2 doped lead dioxide nanocomposites : investigation of structural and optical microscopy of RhB organic dye, Appl. Surf. Sci. 421 (2017) 234–239, http://dx.doi.org/10.1016/j.apsusc.2016.11.149.
[39] C.M. Magdalane, K. Kaviyarasu, J.J. Vijaya, B. Siddhardha, B. Jeyaraj, J. Kennedy, M. Maaza, Evaluation on the heterostructured CeO2/Y2 O3 binary metal oxide nanocomposites for UV/Vis light induced photocatalytic degradation of Rhodamine - B dye for textile engineering application, J. Alloy. Comp. 727 (2017) 1324–1337, http://dx.doi.org/10.1016/j.jallcom.2017.08.209.
[40] K. Kaviyarasu, K. Kanimozhi, N. Matinise, C.M. Magdalane, G.T. Mola, J. Kennedy, M. Maaza, Antiproliferative effects on human lung cell lines A549 activity of cadmium selenide nanoparticles extracted from cytotoxic effects : investigation of bio-electronic application, Mater. Sci. Eng. C 76 (2017) 1012–1025, http://dx.doi.org/10.1016/j.msec.2017.03.210.
[41] C. Peng, Z. Zhang, Nitrate – citrate combustion synthesis of Ce1-xGdxO2-x/2 powder and its characterization, Ceram. Int. 33 (33) (2007) 1133–1136, http://dx.doi.org/10.1016/j.ceramint.2006.03.004.
[42] R.D. Purohit, S. Saha, A.K. Tyagi, Powder characteristics and sinterability of ceria powders prepared through different routes, Ceram. Int. 32 (2006) 143–146, http://dx.doi.org/10.1016/j.ceramint.2005.01.009.
[43] H.D. Prasad, J. Son, B. Kim, H. Lee, J. Lee, A significant enhancement in sintering activity of nanocrystalline Ce0.9Gd0.1O1.95 powder synthesized by a glycine-nitrate-process, Ceram. Process. Res. 11 (2010) 176–183.
[44] K. Ahn, D.S. Yoo, D.H. Prasad, H. Lee, Y. Chung, J. Lee, Role of Multivalent Pr in the Formation and Migration of Oxygen Vacancy in Pr-doped Ceria: Experimental and First-principles Investigations, (2012).
[45] J.R. McBride, K.C. Hass, B.D. Poindexter, W.H. Weber, Raman and x-ray studies of Ce1-xRExO2-y, where RE=La, Pr, Nd, Eu, Gd, and Tb, J. Appl. Phys. 76 (1994) 2435–2441, http://dx.doi.org/10.1063/1.357593.
[46] Z. He, H. Yuan, J.A. Glasscock, C. Chatzichristodoulou, J.W. Phair, A. Kaiser, S. Ramousse, Densification and grain growth during early-stage sintering of Ce0.9Gd0.1O1.95-δ in a reducing atmosphere, Acta Mater. 58 (2010) 3860–3866, http://dx.doi.org/10.1016/j.actamat.2010.03.046.
[47] S.P. Li, J.Q. Lu, P. Fang, M.F. Luo, Effect of oxygen vacancies on electrical properties of Ce0.8Sm0.1Nd0.1O2-δ electrolyte: an in situ Raman spectroscopic study, J. Power Sources 193 (2009) 93–98, http://dx.doi.org/10.1016/j.jpowsour.2008.12.022.
[48] D.H. Prasad, J.W. Son, B.K. Kim, H.W. Lee, J.H. Lee, Synthesis of nano-crystalline Ce0.9Gd0.1O1.95 electrolyte by novel sol-gel thermolysis process for IT-SOFCs, J. Eur. Ceram. Soc. 28 (2008) 3107–3112, http://dx.doi.org/10.1016/j.jeurceramsoc.2008.05.021.
[49] L.P. Kouwenhoven, N.C. Van Der Vaart, a. T. Johnson, W. Kool, C.J.P.M. Harmans, J.G. Williamson, a. a. M. Staring, C.T. Foxon, Single electron charging effects in semiconductor quantum dots, Z. Phys. B Condens. Matter 85 (1991) 367–373, http://dx.doi.org/10.1007/BF01307632.
[50] J.H.F. Scott-Thomas, S.B. Field, M.A. Kastner, H.I. Smith, D.A. Antoniadis, Conductance oscillations periodic in the density of a one-dimensional electron gas, Phys. Rev. Lett. 62 (1989) 583, http://dx.doi.org/10.1103/PhysRevLett.63.1893.
[51] S.B. Field, M. Kastner, U. Meirav, J.H. Scott-Thomas, D.A. Antonadis, H.I. Smith, S.J. Wind, Conductance oscillations periodic in the density of one-dimensional electron gases, Phys. Rev. B vol. 42, (1990) 3523, http://dx.doi.org/10.1088/1367-2630/9/9/346.
[52] A.A.M. Staring, H. van Houten, C.W.J. Beenakker, C. Foxon, High Magnetic Fields in Semiconductor Physics III, (1990), http://dx.doi.org/10.1007/978-3-642-84408-9 Berlin, He.
[53] H. van Houten, C.W. Beenakker, Comment on “conductance oscillations periodic in the density of a one-dimensional electron gas,”, Phys. Rev. Lett. 63 (1989) 1893.
[54] L.I. Glazman, R.I. Shekhter, Coulomb oscillations of the conductance in a laterally confined heterostructure, J. Phys. Condens. Matter 1 (1989) 5811–5815, http://dx.doi.org/10.1088/0953-8984/1/33/027.
[55] S. Dogra, J. Singh, N. Dilawar Sharma, K. Samanta, H.K. Poswal, S.M. Sharma, A.K. Bandyopadhyay, Phase progression via phonon modes in lanthanide dioxides under pressure, Vib. Spectrosc. 70 (2014) 193–199, http://dx.doi.org/10.1016/j.vibspec.2013.12.005.
[56] S. Medisetti, J. Ahn, S. Patil, A. Goel, Y. Bangaru, G.V. Sabhahit, G.U.B. Babu, J.-H. Lee, H.P. Dasari, Synthesis of GDC electrolyte material for IT-SOFCs using glucose & fructose and its characterization, Nano-Structures & Nano-Objects 11 (2017) 7–12, http://dx.doi.org/10.1016/j.nanoso.2017.05.009.
[57] S. Pooneh, V. Chris, S. Farida, Trap level measurements in wide band gap materials by thermoluminescence, Luminescence-an-Outlook-on-the-Phenomena-and-Their-Applications, 2016, http://dx.doi.org/10.5772/65306.
[58] Y. Liu, L. Fan, Y. Cai, W. Zhang, B. Wang, B. Zhu, Superionic conductivity of Sm 3+, Pr 3+, and Nd 3+ triple-doped ceria through bulk and surface two-step doping approach, ACS Appl. Mater. Interfaces 9 (2017) 23614–23623, http://dx.doi.org/10.1021/acsami.7b02224.
[59] K. Venkataramana, C. Madhuri, Y. Suresh Reddy, G. Bhikshamaiah, C. Vishnuvardhan Reddy, Structural, electrical and thermal expansion studies of tri-doped ceria electrolyte materials for IT-SOFCs, J. Alloy. Comp. 719 (2017) 97–107, http://dx.doi.org/10.1016/j.jallcom.2017.05.022.